Journal of
Materials Chemistry C

ROYAL SOCIETY
OF CHEMISTRY

PAPER

View Article Online
View Journal

Check for updates

Cite this: DOI: 10.1039/d5tc01349f

Solution-processed antimony-doped IGZTO thin-film transistors exhibiting superior operational stability under extreme environmental conditions†

Eun Jin Park,[ab] Bu Kyeong Hwang,[a] Bo Ram Lee,[a] In Pyo Park,[a] Hyun Sung Jung,[a] Min-Kyu Son,[a] Hyeon Jin Jung,*[a] Pung Keun Song*[b] and Soo Won Heo*[a]

Received 30th March 2025,
Accepted 10th July 2025

DOI: 10.1039/d5tc01349f

rsc.li/materials-c

Amorphous oxide semiconductors (AOSs) have been widely utilized in display technologies due to their high carrier mobility, excellent uniformity, and low off currents. Conventional vacuum processing is limited by the high production costs and process complexity. The solution-based process offers a promising alternative but still faces challenges like low film density and instability. In this study, we propose Sb-doped indium–gallium–zinc–tin oxide (Sb:IGZTO) as an active layer material for solution-processed thin-film transistors (TFTs) to achieve simultaneous improvements in performance and stability. Sb^{5+} acts as a mobility enhancing dopant while also serving as an oxygen bonding agent, effectively suppressing oxygen vacancy (V_O) formation, thereby improving both the electrical characteristics and environmental stability of the TFTs. The fabricated Sb:IGZTO TFT(3%) exhibited a mobility of 16.43 $cm^2\ V^{-1}\ s^{-1}$, a subthreshold swing value of 0.374 V dec^{-1}, and on/off ratio of 1.67×10^6. Furthermore, the devices demonstrated stable operation under various bias stress conditions. Notably, the Sb:IGZTO TFTs demonstrated excellent long-term stability retaining approximately 74.98% of their initial mobility after 90 days conducted at 85% relative humidity and 85 °C without additional passivation. These findings validate Sb^{5+} doping as an effective strategy to mitigate the trade-off between performance and stability in solution-processed oxide semiconductors.

1. Introduction

Amorphous oxide semiconductors (AOSs) have garnered significant attention in electronic and display technologies due to their high carrier mobility, which arises from the isotropic overlap of the metal ns orbitals.[1] In addition to their high mobility, AOSs offer excellent uniformity, low leakage current, and superior electrical stability,[2,3] making them ideal for high resolution large-area displays such as organic light emitting diodes and micro-light-emitting diodes.[4] Furthermore, AOSs have shown promise for advanced applications including artificial intelligence semiconductors and next-generation memory circuits.[5] The expanding market for extended reality, including virtual reality and augmented reality, has driven the demand for ultra-high-resolution micro displays.[6] Consequently, the demand for and applications of AOS-based technologies are expected to increase.

Currently, vacuum based sputtering techniques dominate the fabrication of AOS devices because of their ability to produce films with low defect densities and excellent electrical characteristics.[7,8] However, these methods require expensive vacuum equipment and involve complex processes, thereby posing challenges for large-area mass production.[9] In contrast, solution based processing has emerged as a cost effective alternative that eliminates the need for vacuum systems, enabling high-throughput manufacturing and large-area device fabrication using simpler procedures.[10] Additionally, solution processing offers greater flexibility in composition control, allowing precise manipulation of metal oxide combinations to optimize device performance.[11]

From the perspective of AOS materials, oxygen vacancy (V_O) plays a two-faced role in the electrical properties of devices. V_O can act as a shallow donor, providing free electrons that contribute to enhanced carrier mobility.[12] However, V_O can also function as an intrinsic defect, negatively impacting the device stability. An excessive concentration of V_O can lead to excessive electron accumulation, exacerbating the threshold voltage (V_{th}) shifts under bias stress and resulting in electrical instability.[13] Furthermore, solution processed thin films exhibit lower molecular density than their vacuum processed counterparts, leading to the retention of impurities such as hydroxyl group (OH^-) and carbon, which originate from the precursor. These

---

[a] Nano Convergence Materials Center, Korea Institute of Ceramic Engineering and Technology (KICET), Soho-ro, Jinju 52851, Gyeongsangnam-do, Republic of Korea. E-mail: laser02hj@kicet.re.kr, soowon.heo@kicet.re.kr

[b] Department of Materials Science and Electronics Engineering, Pusan National University, Busan 46241, Republic of Korea. E-mail: pksong@pusan.ac.kr

† Electronic supplementary information (ESI) available. See DOI: https://doi.org/10.1039/d5tc01349f

residual impurities introduce additional defects, ultimately compromising film quality.[15]

Environmental driving conditions also significantly influence the stability of AOS devices.[16,17] Adsorbed H_2O molecules serve as acceptor-like traps, leading to V_{th} shifts and instability.[18] While passivation layers are commonly employed to mitigate these effects,[19] they increase production complexity and costs. Accordingly, the development of materials that can enhance stability without additional processing is essential. Although solution processing presents significant challenges, its various advantages necessitate further optimization through material improvements and continuous research.

To address these challenges, various doping strategies have been investigated from the material perspective. For example, magnesium doping has been shown to modulate the V_O density and improve the stability of amorphous-indium–gallium–zinc-oxide (a-IGZO).[20] Similarly, nitrogen doping enhances the electrical properties and stability of IGZO,[21] whereas yttrium doping effectively regulates the carrier concentration and electrical stability.[22] Additionally, fluorine plasma treatment has been reported to increase the carrier concentration, mobility, and thermal stability of IGZO films.[23] Among these approaches, Sn doping IGZO(IGZTO) introduces Sn^{4+} with an electron orbital (5s orbital) similar to In^{3+}, contributing to the conduction path, increasing the mass density within the thin film, and enhancing electron mobility.[24–26] As a result, IGZTO exhibits high mobility, even when fabricated *via* solution processing. However, conventional thermal treatments of IGZTO often result in negative V_{th} shifts,[27] leading to increased operating voltages and power consumption, which hinder their applicability in portable electronic devices. Furthermore, heat dissipation from the backplane can adversely affect the pixel performance and flexible substrates.[28]

In this study, we doped antimony (Sb) into IGZTO through solution processing, resulting in the development of Sb-doped IGZTO (Sb:IGZTO) as an active layer material. The oxidation state of Sb ions, Sb^{5+}, serves two primary functions in enhancing the electrical performance and environmental stability. (i) Optimization of conduction pathways; Sb^{5+} optimizes the conduction pathways, thereby improving the carrier mobility and facilitating more efficient charge transport. (ii) Suppression of V_O; Sb^{5+} effectively suppresses the formation of V_O, contributing to improved device stability.[29] The fabricated Sb:IGZTO TFTs exhibited a high carrier mobility, low SS, favorable on/off ratio, excellent bias, and photo-stress stability. Notably, long-term reliability tests under high relative humidity (85%) and temperature (85 °C) for 90 days without additional passivation revealed that Sb:IGZTO retained approximately 74.98% of its initial mobility. These results underscore the effectiveness of Sb^{5+} doping in overcoming the trade-off between performance and stability.[30]

2. Experimental

2.1 Synthesis of metal oxide solution

The IGZTO solution was synthesized by dissolving indium chloride, gallium nitrate, zinc acetate dihydrate, and tin chloride in 2-methoxyethanol (99.8%) at a molar ratio of 1 : 0.5 : 1 : 0.1. Additionally, antimony chloride was introduced into the IGZTO solution at concentrations of 1, 3, and 5%. All metal precursors and solvents were purchased from Sigma-Aldrich. The precursor solutions were stirred at 80 °C and 700 rpm for 24 h to ensure complete dissolution, which resulted in four different solutions. Based on the molar ratios of the metal precursors, the atomic composition of the IGZTO matrix was calculated as In: 38.45 at%, Ga: 3.82 at%, Zn: 38.43 at%, and Sn: 19.31 at%. The actual Sb atomic concentrations corresponding to nominal doping levels of 1%, 3%, and 5% were estimated to be approximately 0.51 at%, 1.53 at%, and 2.52 at%, respectively. These values were calculated from the input molar ratios of $SbCl_3$ relative to the total metal content.

2.2 Device fabrication

Heavily doped silicon ($P^{++}Si$) with a 100 nm thick SiO_2 layer was employed as the gate electrode and gate insulator, respectively. The SiO_2/Si substrates were sequentially cleaned with acetone, isopropyl alcohol, detergent, and deionized water for 10 min each. The cleaned substrates were then dried on a hotplate at 150 °C for 10 min to remove organic residues, followed by an ultraviolet ozone treatment (AC-16, Ahtech) for 10 min to enhance adhesion. All precursor solutions were filtered through 0.45 μm membrane syringe filters prior to spin-coating. Metal oxide thin films were deposited by spin coating at 3000 rpm for 20 s. The coated films were pre-annealed at 150 °C for 10 min to remove residual solvents and subsequently annealed in ambient air at 550 °C for 1 h in a furnace. A lift-off process was used to pattern the active channel, defining a channel width (W) and length (L) of 100 and 80 μm, respectively. Indium tin oxide was deposited as source/drain electrodes *via* magnetron sputtering at a thickness of 100 nm, followed by patterning using a lift-off process.

2.3 Thin film and device characterization

The electrical characteristics and bias stress stability of the fabricated TFTs were evaluated using a HP 4145B semiconductor parameter analyzer (Hewlett-Packard) under ambient air and dark conditions. The transfer characteristics were measured by sweeping the gate voltage from −40 V to 40 V in 0.2 V steps. For the bias thermal stress tests, heating was performed using a MST-1000H hot chuck controller (MSTECH), while bias illumination stress tests were conducted using a FOK-100 W switching mode power supply (Fiber Optic Korea). The carrier concentration, Hall mobility, and resistivity of IGZTO and Sb:IGZTO thin films were determined using a Hall measurement system (HMS-5000, Ecopia) at room temperature. The cross-sectional image of Sb:IGZTO(3%) TFT was measured using transmission electron microscopy (TEM, JEM-4010, JEOL). The surface roughness was analyzed by atomic force microscopy (AFM, NX20 300 nm, Park Systems). The chemical compositions of the IGZTO and Sb:IGZTO films were analyzed *via* X-ray photoelectron spectroscopy (XPS, Al Kα 1486.68 eV, NEXSA XPS, Thermo Fisher Scientific), with binding energies calibrated using the C 1s peak at 284.6 eV. The optical bandgap energies of the films were evaluated using UV-visible spectroscopy (V-670, Jasco) and analyzed using Tauc plots. The crystalline structure of the IGZTO and Sb:IGZTO thin films were analyzed using grazing incidence X-ray diffraction (D8 Advance A25 Plus, Bruker). The linear-region field-effect mobility (μ_{lin}) of the fabricated TFTs was calculated using the following equation:

$$\mu_{\text{FE}} = \frac{g_{\text{m}}L}{WC_{\text{ox}}V_{\text{D}}} \tag{1}$$

$$\mu_{\text{lin}} = \frac{L}{WC_{\text{ox}}V_{\text{D}}}\left(\frac{\delta I_{\text{D}}}{\delta V_{\text{G}}}\right) \tag{2}$$

where g_{m} denotes the transconductance obtained by deriving the I_{DS}–V_{GS} curve, C_{ox} denotes the conductance per unit area, and L and W denote the channel length (80 μm) and width (100 μm), respectively. SS was obtained using the following equation:

$$\text{SS} = \left(\frac{\text{d}\log(I_{\text{DS}})}{\text{d}V_{\text{GS}}}\right)^{-1} \tag{3}$$

where I_{DS} denotes the drain-to-source current and V_{GS} denotes the gate bias. The interface trap density (D_{it}) was calculated using the following equation:

$$D_{\text{it}} = \frac{C_{\text{ox}}}{q}\left(\frac{q\text{SS}}{kT\ln 10} - 1\right) \tag{4}$$

where q is the electron charge, k is the Boltzmann constant, T is the absolute temperature, and C_{ox} is the conductance per unit area.

2.4 Long-term stability test under extreme environmental conditions

All TFT devices used for the long-term environmental stability test were fabricated without any passivation layer. The environmental test was carried out in a sealed aluminum chamber ($20 \times 20 \times 20$ cm^3) maintained at 85 °C and 85% RH relative humidity for 90 days.

3. Results and discussion

Fig. 1a and b and Fig. S1 (ESI†) show the transfer and output characteristics of indium–gallium–zinc–tin oxide (IGZTO) thin-film transistors (TFTs) doped with antimony (Sb) at doping levels of 1, 3, and 5%, respectively. The electrical parameters are listed in Table 1. The pristine IGZTO TFT exhibited the mobility of 13.76 cm^2 V^{-1} s^{-1}, SS value of 0.514 V dec^{-1}, and on/off ratio of 1.30×10^6, respectively. Upon doping with Sb 3%, a significant enhancement in the device performance was observed. Specifically, in Fig. 1a, when the Sb doping level was 3%, a positive shift in the threshold voltage (V_{th}) to +1 V and an increase in the on-current were observed. Additionally, Fig. 1b illustrates the improved output characteristics at Sb doping levels of 3% compared to undoped IGZTO. The Sb:IGZTO(3%) TFT demonstrated a mobility of 16.43 cm^2 V^{-1} s^{-1}, a decreased SS value of 0.374 V dec^{-1}, and an enhanced on/off ratio of 1.67×10^6, corresponding to a 19.40% mobility improvement relative to IGZTO TFTs. In contrast, doping concentrations of 1% and 5% led to reduced mobility values of 12.53 cm^2 V^{-1} s^{-1} and 10.92 cm^2 V^{-1} s^{-1}.

These results can be explained by the difference between the two predominant oxidation states of Sb cations, Sb^{5+} and Sb^{3+}. Sb^{5+}, with a higher oxidation state, acts as a donor[29] near the conduction band, increasing the carrier concentration and enhancing the conductivity. This leads to a higher source/drain current and positive V_{th} shift, thereby improving the output characteristics. Additionally, the high electronegativity of Sb^{5+} (2.05) facilitates strong bonding with oxygen ions, which suppresses the formation of V$_{\text{O}}$ and strengthens the metal–oxygen (M–O) bond network. This reduces the electron trap states, resulting in improved SS and stabilized charge transport pathways, enhancing electrical performance. Conversely, Sb^{3+}, which exhibits a lower oxidation state, functions as an acceptor[29] by capturing free electrons from the conduction band, thereby reducing the carrier concentration. This negatively affects the channel formation, necessitating higher gate voltages and shifting V_{th} negatively, thus degrading the current flow. Moreover, Sb^{3+} introduces defect states that increase electron scattering, leading to reduced mobility and compromising overall electrical performance.

Hall effect measurements were conducted to elucidate the influence of Sb cations on the charge transport mechanism. For Sb:IGZTO(1%), although the carrier concentration and Hall mobility (μ_{Hall}) increased, the TFT mobility decreased compared with that of pristine IGZTO. This discrepancy is attributed to the interplay between the Sb oxidation states and their impact on electron transport and interface characteristics. Specifically, V$_{\text{O}}$ acts as a shallow donor and is one of the primary factors contributing to the increase in electron concentration. However, Sb^{5+} tends to reduce the density of V$_{\text{O}}$ by acting as an oxygen bonding agent. However, the additional electrons generated by Sb^{5+} doping contribute to the conduction band, leading to an increase in carrier concentration. Consequently, the μ_{Hall} was also enhanced compared to IGZTO. Ultimately, the reduction in the Sb:IGZTO(1%) TFT mobility is attributed to the presence of Sb^{3+}. Sb^{3+} forms an acceptor-like state that acts as an electron trap, thereby hindering electron transport. This effect became particularly pronounced when a gate bias was applied to the TFT. While μ_{Hall} reflects the intrinsic physical characteristics of charge transport, TFT mobility is significantly influenced by the interface states and electron traps. The presence of Sb^{3+} increases the density of trap states both at the interface and within the bulk, thereby restricting electron movement under an applied electric field and leading to a decrease in the TFT mobility. Consequently, the interface trap density (D_{it}) of Sb:IGZTO(1%) was measured as 2.62×10^{12} cm^{-2} eV^{-1}, higher than that of IGZTO. As a result, despite the enhancement in μ_{Hall} due to Sb doping, the increase in electron trap states induced by Sb^{3+} and the higher D_{it} contributed to the reduction in TFT mobility.

For Sb:IGZTO(3%), the optimal doping concentration and the donor effect of Sb^{5+} was maximized, while the acceptor effect of Sb^{3+} was minimized. This balance optimized the charge transport path, increasing the carrier concentration to 6.89×10^{18} cm^{-3} and enhancing μ_{Hall} to 5.49 cm^2 V^{-1} s^{-1}. The resulting percolation transport pathway facilitated efficient electron movement, leading to a TFT mobility of 16.43 cm^2 V^{-1} s^{-1}. Whereas, for

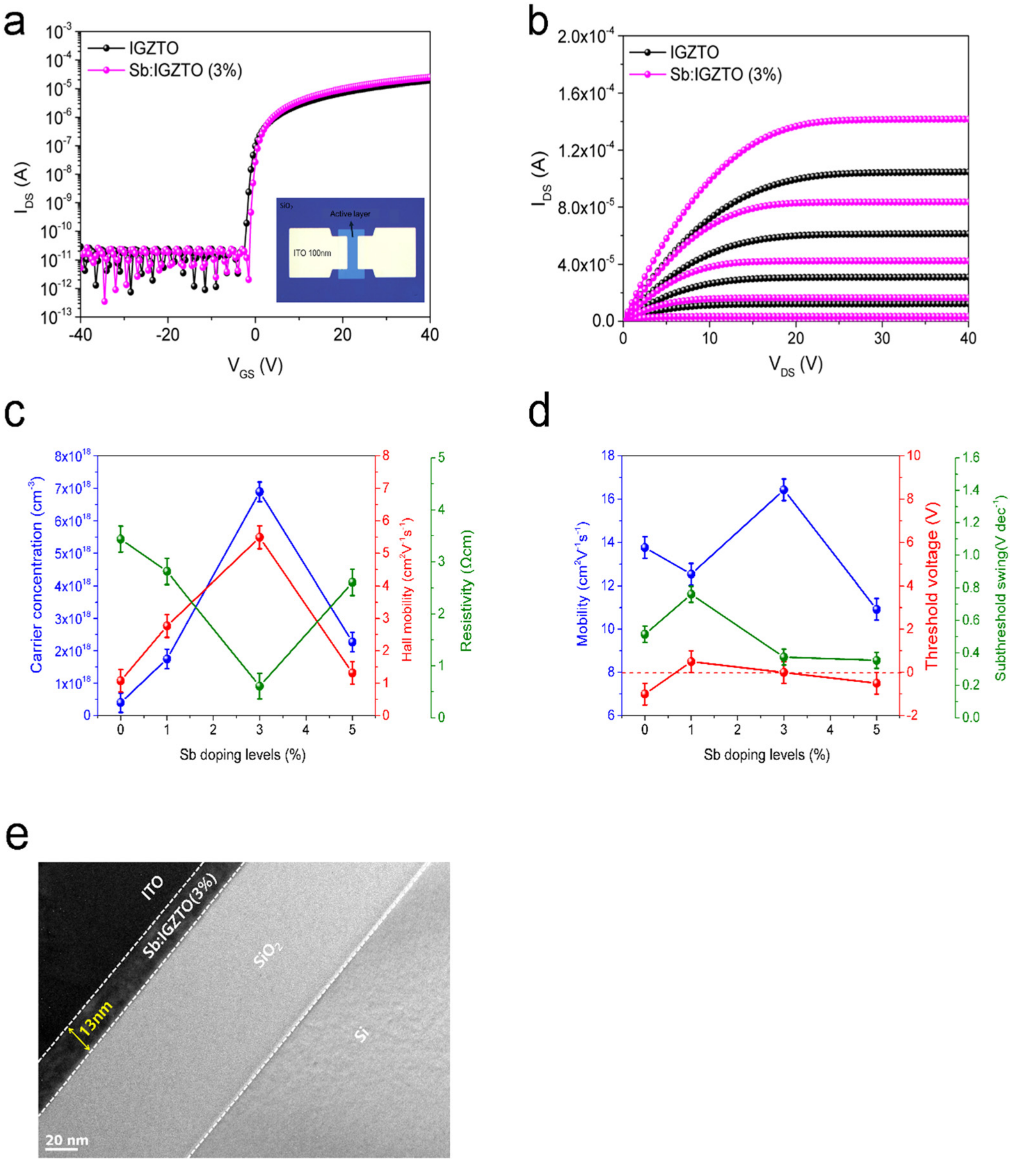

Fig. 1 (a) Transfer (I_{DS}–V_{GS}) characteristics of IGZTO and Sb:IGZTO(3%) TFTs. The inset shows the optical microscope images of the Sb:IGZTO(3%) TFT. (b) Output (I_{DS}–V_{DS}) characteristics of IGZTO and Sb:IGZTO(3%) TFTs. (c) Hall effect measurement characteristics (carrier concentration, Hall mobility, and resistivity) of IGZTO thin films with various (1, 3, and 5%) Sb doping levels. (d) Electrical properties (linear-region field-effect mobility, threshold voltage, and subthreshold swing) of IGZTO TFTs with various Sb doping levels. The average and standard deviation values for all parameters were obtained from measurements of 10 separate devices. (e) Cross-sectional HR-TEM images of Sb:IGZTO(3%) TFT.

Sb:IGZTO(5%), a notable decline in carrier concentration to 2.27×10^{18} cm^{-3} and μ_{Hall} to 1.32 cm^2 V^{-1} s^{-1} was observed, resulting in decreased TFT mobility. This deterioration is attributed to excessive Sb^{3+} formation, which introduces electron capture traps and reduces the conduction band carrier concentration. Moreover, the strong oxygen binding effect of Sb^{5+} excessively suppressed V_O formation, limiting the supply of free electrons and negatively affecting the electrical performance. Additionally, high Sb doping levels induced increased trap-induced scattering, further degrading mobility. Meanwhile, the increased proportion of Sb^{3+} species

Table 1 Electrical parameters of IGZTO TFT with and Sb:IGZTO TFTs various dopant Sb doping levels

	Mobility [cm^2 V^{-1} s^{-1}]	V_{th} [V]	SS [V dec^{-1}]	On/off ratio [$\times 10^6$]	D_{it} [$\times 10^{12}$, cm^{-2} eV^{-1}]
IGZTO	13.76	−1	0.514	1.30	1.70
Sb:IGZTO(1%)	12.53	0.5	0.761	1.12	2.62
Sb:IGZTO(3%)	16.43	0	0.374	1.67	1.18
Sb:IGZTO(5%)	10.92	−0.5	0.354	1.18	1.10

at higher doping concentrations led to the formation of deep-level traps, which acted as scattering centers that hinder the free movement of electrons. This consequently induced trap-related scattering, thereby degrading carrier mobility. Notably, the Hall mobility of the 5% Sb-doped IGZTO film exhibited a significant decline, despite the reduced carrier concentration. Furthermore, band-edge state analysis revealed that this sample exhibited the highest proportion of deep states (77.9%) among all doping conditions, supporting the dominance of deep trap-induced scattering as the primary degradation mechanism. Accordingly, the observed reduction in mobility was attributed not to conventional carrier–carrier scattering, but rather to scattering arising from deep-level trap states. Interestingly, despite the reduced carrier concentration of 2.27×10^{18} cm^{-3} in the Sb:IGZTO (5%) sample, a negative shift in threshold voltage (V_{th}) to −0.5 V was observed. This seemingly counter-intuitive behavior, observed in parallel with the degradation in carrier transport, is attributed to the increased Sb^{3+} content (8.12%), which facilitates the formation of deep-level trap states and causes Fermi level pinning near the conduction band minimum.[31] Consequently, electron accumulation is enhanced under lower gate bias, resulting in earlier channel formation and a negative V_{th} shift. Although the magnitude of the shift is relatively small, this result underscores that Sb induced defect-state modulation can play a critical role in tuning device operation beyond conventional carrier control.

At an optimal Sb concentration of 3%, the electron donation effect of Sb^{5+} was maximized, leading to a significant increase in the carrier concentration and mobility. This results in an enhanced on-state current and reduced off-state leakage, thereby improving the on/off current ratio. In contrast, at 5% Sb doping, the increased presence of Sb^{3+} introduces electron capture traps and structural distortions, leading to enhanced charge scattering and significant mobility degradation. Fig. 1e presents a high-resolution cross-sectional TEM image of the Sb:IGZTO(3%) TFT. Based on the TEM analysis, the thickness of the active layer was confirmed to be approximately 13 nm (±1 nm). Furthermore, no significant thickness variation was observed among the films, regardless of the Sb concentrations.

To further understand the role of Sb oxidation states in IGZTO, X-ray photoelectron spectroscopy (XPS) analysis was conducted. The XPS results reveal the chemical states of Sb and their impact on the electrical properties of Sb:IGZTO. A detailed analysis of the correlation between the Sb oxidation states and electrical properties will be discussed later.

Fig. 2 presents the bias stress stability test results of IGZTO and Sb:IGZTO(3%) TFTs under the conditions of $V_{\text{GS}} = \pm 10$ V and $V_{\text{DS}} = 1.1$ V. The illumination intensity was fixed at 1000 lux, and the temperature was set to 60 °C. The subfigures are organized as follows: (a) and (b) illustrate the ΔV_{th} variations under positive bias stress (PBS), (c) and (d) under negative bias stress (NBS), (e) and (f) under positive bias temperature stress

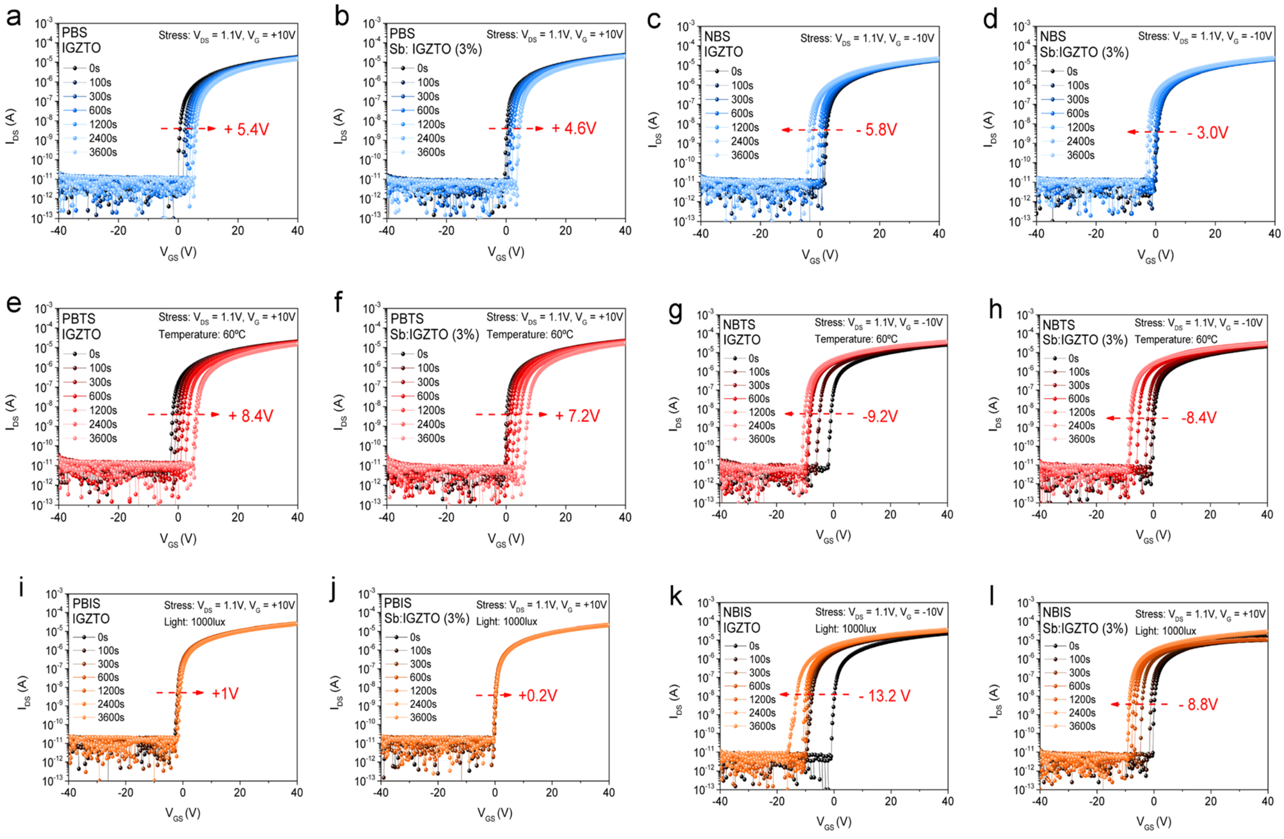

Fig. 2 (a) and (b) Positive bias stress, (c) and (d) negative bias stress, (e) and (f) positive bias temperature stress, (g) and (h) negative bias temperature stress, (i) and (j) positive bias illumination stress, and (k) and (l) negative bias illumination stress test for the IGZTO TFT and Sb:IGZTO(3%), respectively.

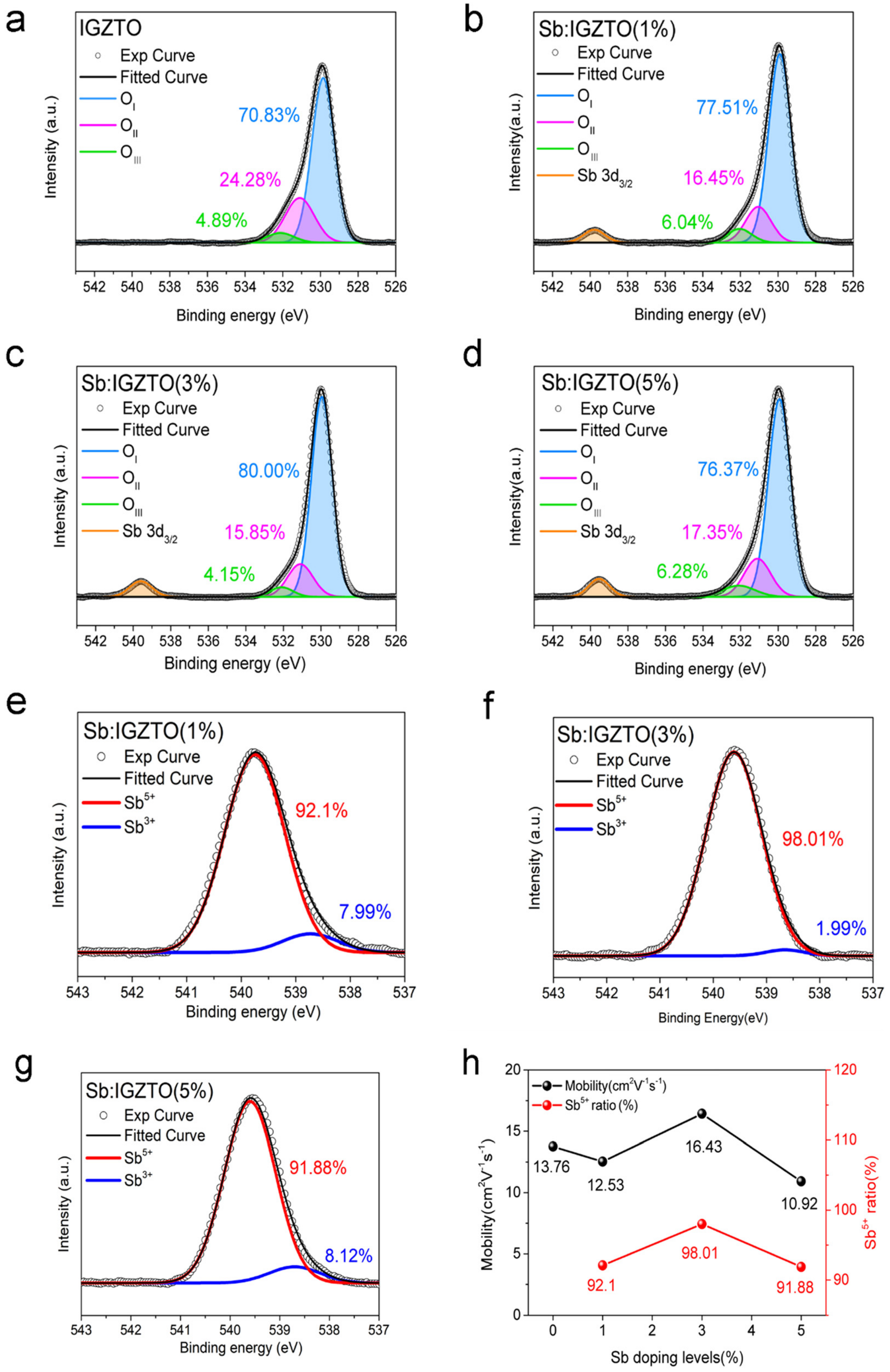

Fig. 3 O 1s XPS and their deconvolution results for the (a) IGZTO film, and the IGZTO films with (b) Sb: 1%, (c) Sb: 3%, and (d) Sb: 5%, respectively. Sb 3d$_{3/2}$ XPS deconvolution results for (e) Sb: 1%, (f) Sb: 3%, and (g) Sb: 5%, respectively. (h) The variation in mobility of the Sb:IGZTO TFTs with different doping levels according to the Sb^{5+} ratio.

(PBTS), (g) and (h) under negative bias temperature stress (NBTS), (i) and (j) under positive bias illumination stress (PBIS), and (k) and (l) under negative bias illumination stress (NBIS). Under PBS and NBS conditions, the ΔV_{th} values of the IGZTO TFTs were measured to be +5.4 V and −5.8 V, respectively (Fig. 2c and d). In contrast, the ΔV_{th} values of the Sb:IGZTO(3%) TFTs decreased to +4.6 V and −3.0 V, indicating a reduction of 14.81% under PBS and 48.28% under NBS. These results suggest that Sb doping effectively enhances the bias stress stability of the IGZTO TFTs. A similar trend was observed under PBTS and NBTS conditions (Fig. 2e–h). For the IGZTO TFTs, ΔV_{th} values of +8.4 V and −9.2 V were observed for the IGZTO TFTs under PBTS and NBTS, respectively. In comparison, the Sb:IGZTO(3%) TFTs exhibited ΔV_{th} values of +7.2 V and −8.4 V, corresponding to improvements of 14.29% and 8.70%, respectively. Fig. 2i–l show the ΔV_{th} variations under PBIS and NBIS conditions. Under PBIS, the IGZTO TFTs exhibited a ΔV_{th} of +1.0 V, whereas the Sb:IGZTO(3%) TFTs exhibited a significantly reduced ΔV_{th} of +0.2 V, representing an 80% decrease. Under NBIS conditions, the IGZTO TFTs exhibited a ΔV_{th} of −13.2 V, while Sb:IGZTO(3%) TFTs showed a reduced ΔV_{th} of −8.8 V, indicating a 33.33% decrease. These findings highlight the superior stability of the Sb:IGZTO(3%) TFTs under illumination stress.

The positive shift of ΔV_{th} under PBS can be attributed to the neutralization of accumulated electron carriers by converting deep V_O states into shallow V_O^{2+} states, as described by the reaction $[V_O^{2+} + 2e^- \rightarrow V_O]$. Conversely, the negative shift under NBS can be explained by the reverse reaction $[V_O \rightarrow V_O^{2+} + 2e^-]$, which becomes energetically favorable as the quasi-Fermi level decreases under NBS conditions, promoting the transition from V_O to V_O^{2+}.[32] Under PBTS, the shallow donor V_O^{2+} injects electrons into the gate insulator due to the combined effects of positive gate bias and elevated temperature. This process leads to the neutralization of defects through the transition from V_O^{2+} to V_O, resulting in a positive shift in ΔV_{th}. In contrast, under the NBTS, hole accumulation occurs in the channel due to the applied gate bias. These holes interacted with oxygen related defects, facilitating negative shifts in ΔV_{th}. Specifically, holes can be trapped by V_O or M(metal)–OH, forming hole traps within the channel, which accelerates the negative shift.[33] Under PBIS, a positive gate bias traps electrons at the channel–insulator interface. Illumination ionizes V_O, releasing electrons into the conduction band, thereby increasing the electron concentration in the conduction band. However, at high V_O concentrations, the increased number of electron traps caused a positive shift in ΔV_{th}. Under NBIS, the simultaneous application of a negative gate bias and illumination leads to the photodesorption of oxygen ions adsorbed on the channel surface, releasing free electrons into the conduction band. This increased the electron concentration in the conduction band, resulting in a pronounced negative shift in ΔV_{th}.[33–35]

The superior stability of the Sb:IGZTO(3%) TFT under various stress conditions is attributed to the role of Sb^{5+}(2.05) as an oxygen bonding agent, which strongly bonds with oxygen ions in the IGZTO system because of its high electronegativity. This effectively suppressed the formation of V_O and impurity-related trap sites, such as OH^-. Consequently, the Sb:IGZTO(3%) TFTs exhibited enhanced stability compared to IGZTO TFTs under bias, temperature, and illumination stress conditions.

XPS analysis was conducted to investigate the chemical state changes and their impact on the electrical properties and stability of IGZTO and Sb:IGZTO thin films (Fig. 3). The O 1s spectra of IGZTO and Sb-doped IGZTO films (1%, 3%, and 5% Sb doping) were obtained after annealing at 550 °C, and the photoelectron binding energy was calibrated using the C 1s peak corresponding to C–C bonding (284.6 eV). The O 1s spectra were deconvoluted using Gaussian fitting into three primary peaks: metal–oxygen (M–O) bonding (529.8 eV ± 0.05), oxygen vacancy (V_O, 531.1 eV ± 0.05), and impurities such as OH^- (532.1 eV ± 0.05),[36] labeled as O_I, O_{II}, and O_{III},[14] respectively. An additional Sb $3d_{3/2}$ peak was observed at 539.6 eV (Fig. 3b–d).[36] XPS analysis revealed that as the Sb doping concentration increased, the Sb peak intensity gradually intensified, indicating the effective incorporation of Sb ions into the IGZTO system.[29] The corresponding quantitative variations in oxidation states are summarized in Table 2.

The Sb:IGZTO films exhibited a significant reduction in V_O density compared to pristine IGZTO. For example, the O_{II} ratio in Sb:IGZTO(3%) films decreased from 24.28% in IGZTO to 15.85%, demonstrating effective suppression of V_O formation. These findings align with the improved electrical stability observed in the bias stress tests, suggesting that Sb doping effectively mitigated the formation of defect states responsible for electrical degradation.

These changes in the electrical properties can be explained by the roles of Sb^{5+} and Sb^{3+}. In metal oxide systems doped with Sb, Sb^{3+} and Sb^{5+} are likely to act as acceptors and donors, respectively. Fig. 3e–g show the XPS spectra of the Sb $3d_{3/2}$ state in the Sb-doped IGZTO films. The spectra were deconvoluted into two peaks observed at 538.7 eV for Sb^{3+} and 539.6 eV for Sb^{5+}, respectively.[29] Sb^{5+}, having a high oxidation state, acts as a donor in oxygen bonding, supplying electrons to the conduction band, thereby increasing the carrier concentration and mobility. Additionally, Sb^{5+} serves as an effective oxygen bonding agent, suppressing V_O formation and strengthening M–O bonding, which reduces the trap states. In contrast, Sb^{3+}, which has a lower oxidation state, acts as an acceptor, capturing free electrons from the conduction band and reducing carrier concentration. Sb^{3+} also forms defect states that hinder electron movement, leading to a decreased mobility and degraded electrical properties.

In the Sb:IGZTO(1%) film (Fig. 3b and e), the presence of Sb^{3+} (7.99%) resulted in the formation of electron-trapping states, which reduced the stability of the device. This was

Table 2 Variations in the oxidation states of the different Sb:IGZTO films as calculated from the deconvolution of O 1s and Sb $3d_{3/2}$ level in the resulting XPS spectra

Metal oxide film	Sb doping levels [%]	O 1s			Sb $3d_{3/2}$	
		O_I [%]	O_{II} [%]	O_{III} [%]	Sb^{5+} [%]	Sb^{3+} [%]
IGZTO	0	70.83	24.28	4.89	N/A	N/A
	1	77.51	16.45	6.04	92.1	7.99
	3	80.00	15.85	4.15	98.01	1.99
	5	76.37	17.35	6.28	91.88	8.12

evidenced by an increase in the O_I ratio from 70.83% in IGZTO to 77.51% and a corresponding decrease in the O_{II} ratio from 24.28% to 16.45%, indicating the suppression of V_O formation. However, the O_{III} ratio increased from 4.89% to 6.04%, suggesting the presence of structural defects. These results imply that the presence of Sb^{3+} disrupts the percolation path and increases the trap states and charge scattering, leading to reduced mobility. In contrast, the Sb:IGZTO (3%) film (Fig. 3c and f) exhibited the highest Sb^{5+} fraction (98.01%), maximizing its role as a donor and significantly enhancing carrier mobility. The O_I ratio increased to 80.00%, indicating strengthened M–O bonding, whereas the O_{II} ratio decreased to 15.85%, effectively suppressing V_O formation. In addition, the O_{III} ratio decreased to 4.15%, thus minimizing the trap states. This enhancement in structural stability suggests the formation of a continuous percolation path, leading to an increased μ_{Hall} and improved electrical performance. Thus, the 3% Sb doping concentration optimizes the charge transport pathway, effectively balancing electron donation and defect suppression, resulting in high mobility, low SS, and improved environmental stability. However, in the Sb:IGZTO(5%) film (Fig. 3d and g), the Sb^{3+} fraction increased sharply to 8.12%, leading to the formation of electron-trapping states and a consequent reduction in the carrier concentration. XPS analysis revealed a decrease in the O_I ratio to 76.37% and an increase in the O_{II} ratio to 17.35%, indicating increased V_O formation. This suggests that excessive Sb doping induces structural distortions and increases carrier scattering, leading to a decreased mobility of 10.92 $cm^2\ V^{-1}\ s^{-1}$. The increase in Sb^{3+} introduces defect states that act as charge trapping centers, disrupting the percolation path and reducing charge transport efficiency. Furthermore, a negative V_{th} shift to −0.5 V was observed due to the reduced carrier concentration, indicating degraded electrical properties.

XPS analysis provides a comprehensive understanding of the correlation between Sb doping concentration and the electrical performance of IGZTO thin films. At an optimal Sb doping concentration of 3%, Sb^{5+} is predominant, acting as a donor to enhance carrier concentration and mobility while effectively suppressing V_O formation and minimizing trap states. In contrast, at 1% Sb doping, the presence of Sb^{3+} introduces electron-trapping states that limit mobility, whereas at 5% Sb doping, the excessive formation of Sb^{3+} increases charge scattering and structural distortions, leading to mobility degradation. Therefore, the ratio of Sb^{5+} acting as a donor corresponds to the change in mobility (Fig. 3h).

Gaussian fitting was performed to investigate the band edge states below the conduction band minimum (CBM) of the IGZTO and Sb:IGZTO thin films, and the corresponding results are presented in Fig. 4a–d. The optical properties of the films were compared and analyzed, as shown in Fig. S4 (ESI†). In

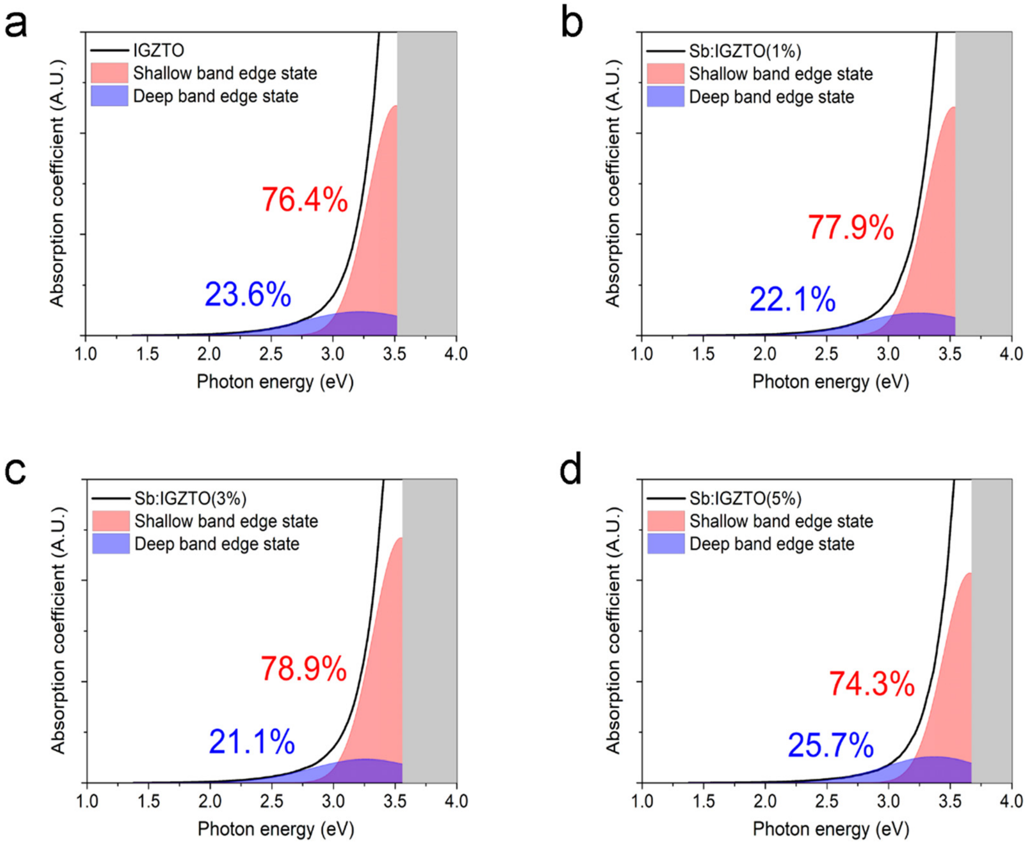

Fig. 4 Band edge state below the conduction band minimum of the (a) IGZTO film, and IGZTO films with (b) Sb: 1%, (c) Sb: 3%, and (d) Sb: 5%, respectively.

n-type metal oxide semiconductors, tail states near the CBM are indicative of defect states within the film, with an increase in the density of electron trap levels within the bandgap correlating with an increase in the absorption coefficient.[38] These defect states can be broadly classified into two categories: shallow band edge states, which are closer to the CBM and are primarily associated with V_O, and deep band edge states, which are located further from the CBM and contribute to charge scattering and electron mobility degradation.[38]

To quantitatively analyze these effects, the shallow band edge states and deep band edge states were distinguished, and their respective ratios were calculated. Typically, an increase in doping concentration leads to an increase in defects and charge scattering, thereby increasing the proportion of deep band edge states. However, in the Sb:IGZTO(1%) and Sb:IGZTO(3%) thin films, a decrease in the proportion of deep band edge states was observed. This phenomenon is attributed to the high electronegativity (2.05) of Sb^{5+} ions, which form strong bonds with oxygen ions in the IGZTO matrix, effectively suppressing V_O formation. In undoped IGZTO thin films, V_O is the primary factor contributing to the formation of deep band edge states. However, with Sb^{5+} doping, V_O formation is suppressed, strengthening M–O bonding and reducing the formation of deep band edge states originating from defect centers. Additionally, Sb^{5+} acts as a donor, increasing the carrier concentration and optimizing the electron transport pathways. Consequently, the reduction in the deep band edge states mitigates charge scattering, thereby enhancing charge transport characteristics.

For the Sb:IGZTO(1%) thin film (Fig. 4b), the proportions of shallow and deep states were 77.9% and 22.1%, respectively. The reduced deep state ratio is attributed to the suppression of V_O formation, as Sb^{5+} acts as an oxygen bonding agent. However, the presence of a small amount of Sb^{3+} ions led to a reduction in mobility. These Sb^{3+} ions form electron trapping sites, increasing the D_{it}, which in turn induces electron trapping and scattering, thereby reducing the actual mobility of TFTs. Consequently, despite the improvement in structural stability due to the suppressed V_O formation, the electron transport pathway was disrupted by the presence of Sb^{3+} induced trap states, resulting in limited mobility enhancement.

In contrast, the Sb:IGZTO(3%) thin film (Fig. 4c) exhibited the highest proportion of shallow states (78.9%) and the lowest proportion of deep states (21.1%). This indicates that at 3% Sb doping, the Sb^{5+} concentration was maximized, leading to an enhanced electron donation effect, while the Sb^{3+} concentration was minimized, thereby reducing electron trapping. Additionally, Sb^{5+} effectively increased the carrier concentration and improved the conductivity by optimizing the percolation pathways for electron transport. As the deep band edge states are reduced, charge scattering is minimized, and mobility and overall electrical performance are improved. Hall effect measurements confirmed that the Sb:IGZTO(3%) thin film exhibited the highest carrier concentration and μ_{Hall}, consistent with the band edge state analysis.

However, in the Sb:IGZTO(5%) thin film (Fig. 4d), the proportion of shallow states decreased to 74.3%, whereas the deep state proportion increased to 25.7%. This increase in deep states is attributed to a higher Sb^{3+} concentration, which introduces electron trapping states and disrupts the percolation path. Consequently, the carrier concentration decreased significantly, leading to a reduction in the electrical conductivity. Additionally, the increased internal charge trapping resulted in a slight decrease in the D_{it} but did not contribute to the overall mobility enhancement. The higher Sb^{3+} content acts as an acceptor, capturing free electrons and thereby reducing the carrier concentration. These analytical results further support the reliability of the earlier electrical properties and stability.

In addition to the bias stress test, the long-term stability of the devices was evaluated under extreme environmental conditions. IGZTO and Sb:IGZTO(3%) TFTs were subjected to 85% relative humidity (RH) at 85 °C for 90 days, and their electrical characteristics were measured daily using a probe station. The mobility measured over 90 days is presented as normalized mobility in Fig. 5a, with a detailed summary provided in Table 3. Additionally, to further assess the potential contribution of surface-related factors to the observed environmental degradation, static water contact angle measurements were performed on both IGZTO and Sb:IGZTO (3%) thin films. The contact angles were found to be comparable, suggesting that Sb incorporation does not significantly affect the surface hydrophobicity. These findings indicate that the difference in long-term stability between the two systems is predominantly governed by intrinsic material property modifications rather than surface energy variations (Fig. S6, ESI†).

After 90 days, the conventional IGZTO TFT exhibited catastrophic degradation, rendering mobility measurements infeasible, whereas the Sb:IGZTO(3%) TFT retained 74.98% of its initial mobility. The initial mobility retention was 74.98% under these extreme conditions, demonstrating superior long-term stability compared to previous studies (Table S1, ESI†). The degradation mechanism of the IGZTO TFT under extreme long-term conditions and the effect of Sb doping on the electrical stability of IGZTO are illustrated in Fig. 5b and c, respectively.

As the IGZTO TFT lacks a dopant that strengthens the M–O bonding, prolonged exposure to extreme environmental conditions (85 °C and 85% relative humidity for 90 days) leads to the breaking of weak M–O bonds and a sharp increase in V_O. Although V_O can initially act as shallow donors and increase carrier concentration, under such extended stress, they may instead function as deep traps or scattering centers. As a result, electrons become trapped and the free carrier density decreases, causing a significant drop in mobility. The increased trap density also contributes to instability in the V_{th} and deterioration of the SS. Furthermore, a sharp rise in the off-current drastically reduces the on/off ratio, eventually rendering the device inoperable.

In the case of the Sb:IGZTO(3%) TFT, the high oxidation state (+5) of Sb^{5+}, which acts as an oxygen binder, strongly bonded M–O and mitigates mobility degradation. Consequently, despite long-term exposure to extreme conditions, V_O gradually increases, exhibiting a stabilization mechanism. Even

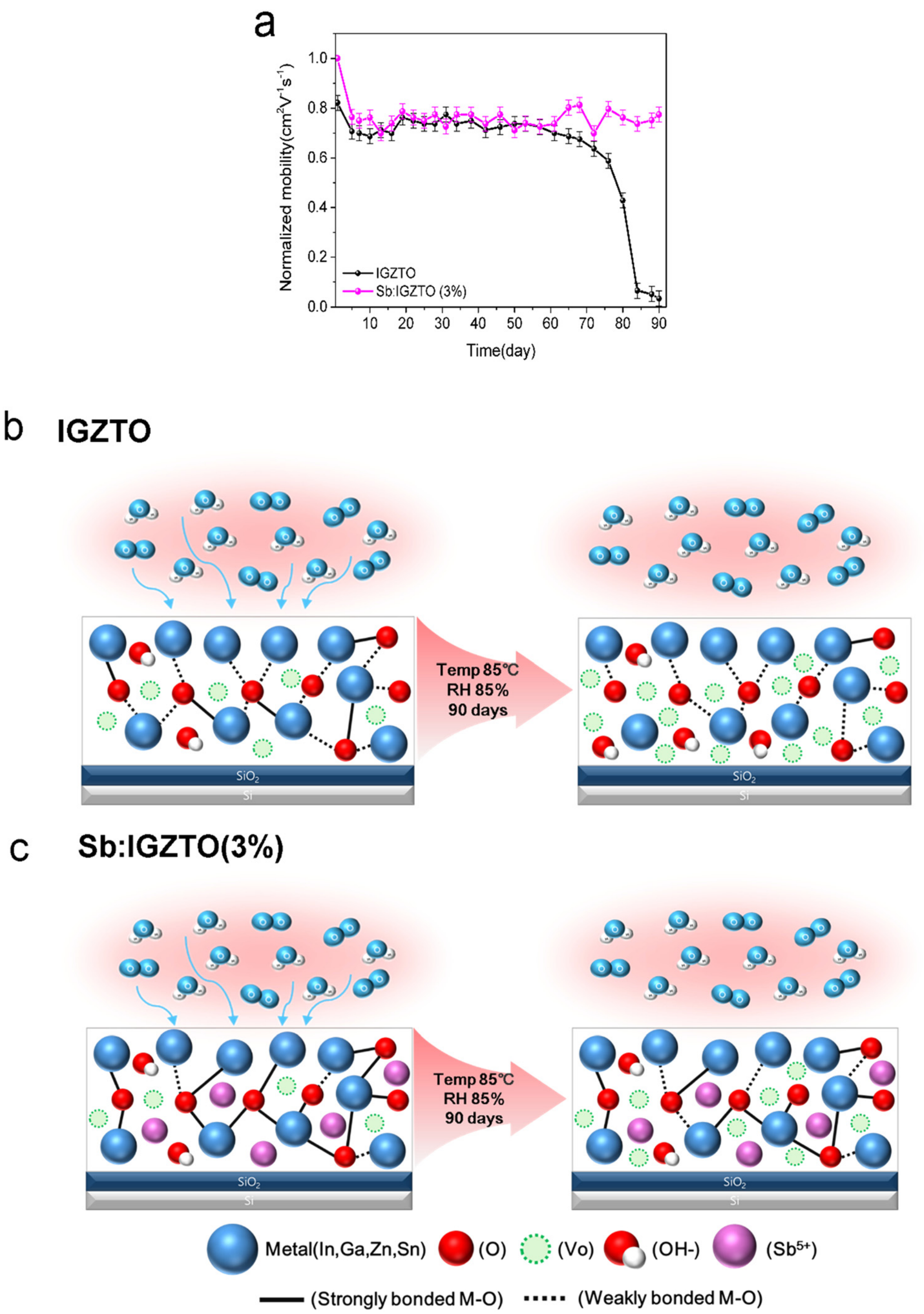

Fig. 5 (a) Normalized mobility of IGZTO TFT and Sb:IGZTO(3%) TFT for 90 days under extreme conditions (RH 85%, 85 °C). Schematic illustrations of changes in (b) the IGZTO and (c) Sb:IGZTO(3%) films after 90 days under extreme conditions (RH 85%, 85 °C).

after 90 days, the device retained 74.98% of its initial mobility with a V_{th} shift of +0.5 V observed. Furthermore, Sb:IGZTO(3%) effectively suppressed OH^- formation, thereby reducing trap-induced degradation and maintaining the increase in SS at a relatively moderate level from 0.374 V dec^{-1} to 0.479 V dec^{-1}. Moreover, by limiting the increase in the off current, the degradation of the on/off ratio was effectively minimized.

To investigate the chemical decomposition mechanism after 90 days under extreme conditions, the O 1s spectra obtained from the XPS analysis of the IGZTO and Sb:IGZTO(3%) films are presented (Fig. 6). The spectra, measured immediately after thermal annealing and long-term storage, were deconvoluted into three primary peaks using Gaussian fitting: M–O bonding (529.8 eV ± 0.05), oxygen vacancy (V_O, 531.1 eV ± 0.05), and OH^- or impurity-related bonding (532.1 eV ± 0.05),[36] labeled as O_I, O_{II}, and O_{III},[14] respectively. Additionally, the Sb $3d_{3/2}$ peak was detected at 539.6 eV[37] in the Sb:IGZTO(3%) film (Fig. 6a–d). After 90 days, the Sb $3d_{3/2}$ peak of the Sb:IGZTO(3%) film decreased compared to its initial state.

Table 3 Electrical parameters of IGZTO TFT and Sb:IGZTO(3%) TFTs immediately after fabrication and after 90 days under extreme conditions (RH 85%, 85 °C temperature)

	Active layer	Mobility [$cm^2\ V^{-1}\ s^{-1}$]	V_{th} [V]	SS [$V\ dec^{-1}$]	On/off ratio [$\times\ 10^6$]	D_{it} [$\times\ 10^{12}$, $cm^{-2}\ eV^{-1}$]
Initial	IGZTO	13.76	−1	0.514	1.30	1.70
	Sb:IGZTO(3%)	16.43	0	0.374	1.67	1.18
After 90 days	IGZTO	N/A	N/A	N/A	N/A	N/A
	Sb:IGZTO(3%)	12.53	0.5	0.479	1.53	1.57

XPS analysis revealed that in the IGZTO film (Fig. 6a and b), the V_O concentration increased by 127.02%, while the M–O bonding decreased by 51.01%, indicating severe chemical decomposition under long-term humidity exposure. The infiltration of H_2O into the active layer weakened the M–O bonding, leading to oxygen loss and an increase in the V_O concentration.

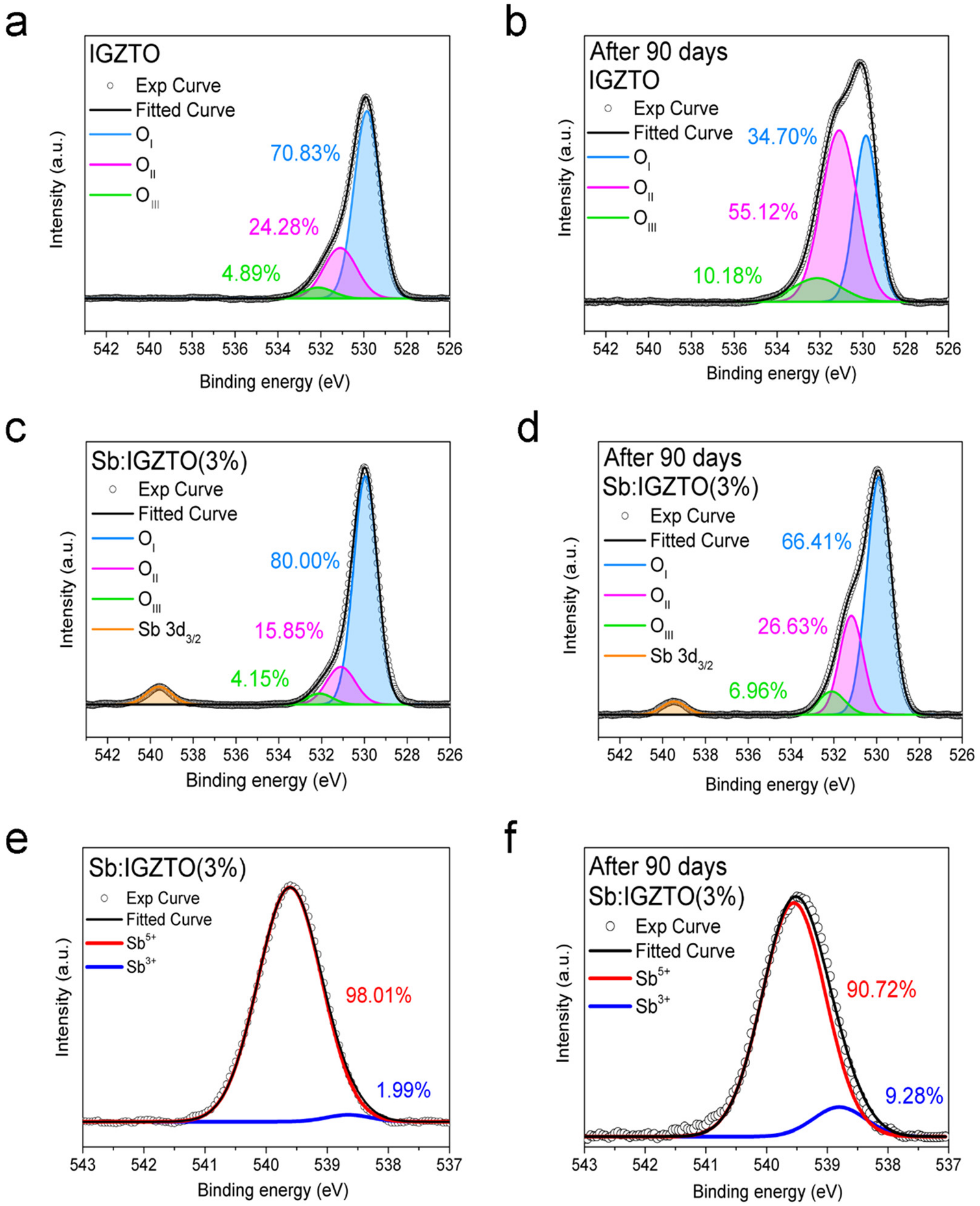

Fig. 6 The XPS results of O 1s and Sb $3d_{3/2}$ show the peak chemical bonding states of (a) and (b) the IGZTO and (c) and (d) the Sb:IGZTO(3%) film initially and after 90 days under extreme conditions (RH 85%, 85 °C), respectively. The XPS results of Sb $3d_{3/2}$ show the peak chemical bonding states of the (e) IGZTO and (f) Sb:IGZTO(3%) film initially and after 90 days under extreme conditions (RH 85%, 85 °C), respectively.

Given the inherently weakly bonded M–O in IGZTO, the material exhibited greater susceptibility to moisture, resulting in a significant increase in V_O and charge imbalance within the active layer. Initially, the increase in V_O enhanced the free electron density and momentarily increased the carrier concentration. However, over extended periods, charge trapping and enhanced electron scattering led to mobility degradation and reliability deterioration. Furthermore, the reduction in M–O bonding induced conduction path irregularities, which severely impacted electron transport. As the V_O density increased, the oxygen deficiency within the device became more pronounced, accelerating V_{th} shifts and long-term stability degradation. Consequently, the IGZTO TFTs experienced severe performance degradation, ultimately reaching a point at which the device became nonfunctional.''

In contrast, the Sb:IGZTO(3%) film exhibited significantly improved stability due to the strong oxygen affinity of Sb^{5+}, which effectively suppressed V_O formation and reinforced M–O bonding. Sb^{5+} strongly interacted with oxygen ions, stabilizing the M–O bonding network and mitigating moisture-induced V_O generation, thereby preventing excessive mobility degradation. Furthermore, Sb^{5+} played a crucial role in suppressing OH^- formation, thereby minimizing charge trapping and mitigating the increase in SS, ultimately enhancing long-term device stability. These effects collectively contributed to preserving the structural integrity of the active layer and maintaining device stability under harsh environmental conditions.

After 90 days, a partial reduction of Sb^{5+} to Sb^{3+} was observed in the Sb:IGZTO (3%) film (Fig. 6e and f). This phenomenon is likely attributed to the formation of oxygen vacancies (V_O) under extreme environmental conditions. Specifically, the breaking of M–O bonding in the oxide matrix generates V_O, which release free electrons and facilitate the reduction of Sb^{5+} to Sb^{3+}. In addition, as the Sb doping concentration increased (*e.g.*, from 3% to 5%), a decrease in the relative fraction of Sb^{5+} and a corresponding increase in Sb^{3+} were observed, as revealed by XPS analysis. This change in oxidation states is interpreted because of a self-compensation mechanism,[39] wherein the formation of acceptor-like Sb^{3+} species becomes energetically favorable to preserve charge neutrality in the IGZTO matrix. These Sb^{3+} species do not contribute free carriers and may act as electron traps, thereby partially offsetting the donor effect of Sb^{5+} and limiting further enhancement in carrier generation. Together, these findings suggest that while Sb^{5+} plays a critical role in reinforcing M–O bonding and suppressing moisture-induced degradation, both environmental reduction and self-compensating oxidation-state transitions may lead to the gradual emergence of Sb^{3+} species, which could potentially affect the long-term electrical performance of Sb-doped IGZTO TFTs.

In conclusion, Sb doping has been demonstrated to be an effective strategy for improving the moisture resistance and long-term electrical stability of IGZTO TFTs. The enhanced reliability is attributed to the dual functionality of Sb^{5+} as an oxygen bonding agent and a donor, which reinforces the chemical structure and electronic states. Furthermore, by reinforcing M–O bonding, Sb^{5+} ions effectively suppress the formation of oxygen vacancies, thereby contributing to improved device reliability. This characteristic may also be exploited to regulate trap-mediated synaptic behaviors in oxide-based neuromorphic devices.[40–42] Accordingly, Sb doping offers not only enhanced electrical stability but also a unified strategy for the development of robust oxide electronics with tunable neuromorphic functionalities.

4. Conclusion

In this study, the impact of Sb doping level on the electrical properties and stability of a-IGZTO TFTs was systematically investigated. Among the evaluated devices, the Sb:IGZTO(3%) TFTs exhibited optimal electrical performance and stability. Sb^{5+} acting as a donor in its high oxidation state, enhanced carrier concentration, and reduced trap states, thereby significantly improving the electrical characteristics. Compared to IGZTO TFTs, Sb:IGZTO(3%) TFTs demonstrated superior performance in terms of mobility, V_{th}, SS, and on/off ratio, which can be attributed to the improved interfacial quality between the channel and gate insulator, as well as the effective suppression of V_O by Sb doping. Bias stress stability evaluations under various conditions (PBS, NBS, PBTS, NBTS, PBIS, and NBIS) revealed that Sb:IGZTO(3%) TFTs exhibited significantly reduced ΔV_{th} shifts compared with IGZTO TFTs, demonstrating excellent durability under different external stimuli, including light exposure and temperature variations. Furthermore, long-term stability tests conducted at RH 85% and 85 °C for 90 days confirmed that Sb:IGZTO(3%) TFTs maintained superior electrical and structural stability compared to IGZTO TFTs. Sb^{5+} played a crucial role in enhancing M–O bonding, suppressing V_O formation, and reducing moisture reactivity, thereby contributing to long-term electrical stability. This study demonstrates that Sb doping is an effective strategy for significantly enhancing the electrical properties and reliability of IGZTO-based TFTs, providing critical insights for the design and fabrication of next-generation electronic devices utilizing oxide semiconductors.

Conflicts of interest

There are no conflicts to declare.

Data availability

The data supporting this article have been included as part of the ESI.†

Acknowledgements

This research was supported by the National Research Foundation of Korea (NRF) funded by the Ministry of Science and ICT (NRF-2020M3H4A3081867) and supported by the Ministry of Trade, Industry and Energy (MOTIE, Korea)(RS-2024-00418877). This work was also supported by the Ceramic Strategic

Research Program (PROJ25033-0-01) through the Korea Institute of Ceramic Engineering & Technology (KICET).

References

1 K. Nomura, H. Ohta, A. Takagi, T. Kamiya, M. Hirano and H. Hosono, *Nature*, 2004, **432**, 488.

2 H. S. Kim, M.-G. Kim, Y.-G. Ha, M. G. Kanatzidis, T. J. Marks and A. Facchetti, *J. Am. Chem. Soc.*, 2009, **131**, 10826.

3 E. Fortunato, P. Barquinha and R. Martins, *Adv. Mater.*, 2012, **24**, 2945.

4 S. Lee, S. H. Lee, N. On and J. K. Jeong, *Ceram. Int.*, 2021, **47**, 6918.

5 M. Dai, Y. Hu, C. Huo, T. J. Webster and L. Guo, *Int. J. Nanomed.*, 2019, **14**, 5691.

6 L. Zhang, H. Yu, W. Xiao, C. Liu, J. Chen, M. Guo, H. Gao, B. Liu and W. Wu, *Electronics*, 2022, **11**, 960.

7 G. Goncalves, E. Elangovan, P. Barquinha, L. Pereira, R. Martins and E. Fortunato, *Thin Solid Films*, 2007, **515**, 8562.

8 J. Lee, J. Jin, S. Maeng, G. Choi, H. Kim and J. Kim, *ACS Appl. Electron. Mater.*, 2022, **4**, 1800.

9 Z. Han, J. Han and A. Abliz, *Appl. Surf. Sci.*, 2024, **648**, 158995.

10 K.-M. Jung, J. Oh, H. E. Kim, A. Schuck, K. Kim, K. Park, J.-H. Jeon, S.-Y. Lee and Y.-S. Kim, *J. Phys. D: Appl. Phys.*, 2020, **53**, 355107.

11 C. Glynn and C. O'Dwyer, *Adv. Mater. Interfaces*, 2017, **4**, 1600610.

12 H.-W. Yeon, S.-M. Lim, J.-K. Jung, H. Yoo, Y.-J. Lee, H.-Y. Kang, Y.-J. Park, M. Kim and Y.-C. Joo, *NPG Asia Mater.*, 2016, **8**, e250.

13 H.-K. Noh, K. J. Chang, B. Ryu and W.-J. Lee, *Phys. Rev. B: Condens. Matter Mater. Phys.*, 2011, **84**, 115205.

14 H. Kim, S. Maeng, S. Lee and J. Kim, *ACS Appl. Electron. Mater.*, 2021, **3**, 1199.

15 W. Cai, M. Li, H. Li, Q. Qian and Z. Zang, *Appl. Phys. Lett.*, 2022, **121**, 062108.

16 J. K. Jeong, H. W. Yang, J. H. Jeong, Y.-G. Mo and H. D. Kim, *Appl. Phys. Lett.*, 2008, **93**, 123508.

17 P.-T. Liu, Y.-T. Chou and L.-F. Teng, *Appl. Phys. Lett.*, 2009, **95**, 233504.

18 D. Kim, S. Yoon, Y. Jeong, Y. Kim, B. Kim and M. Hong, *Appl. Phys. Express*, 2012, **5**, 021101.

19 M. H. Kang, J. Armitage, Z. Andaji-Garmaroudi and H. Sirringhaus, *Adv. Sci.*, 2021, **8**, 2101502.

20 C.-H. Wu, S.-N. Kuo, Y.-M. Chen, K.-M. Chang, Y. Yang and A. Chin, *2020 IEEE Eurasia Conference on IOT, Communication and Engineering (ECICE)*, 2020, pp. 121–124.

21 H. Xiong, L. Fang, F. Wu, D. Liu, Z. Yuan, G. Liu, S. Zhang, H. Zhang, W. Li, P. Yu and C. Tong, *SID Int. Symp. Dig. Tech. Pap.*, 2023, **54**, 90.

22 S. Cho, S. Kim, D. Kim, M. Yi, J. Byun and P. Song, *Coatings*, 2019, **9**, 44.

23 J. G. Um and J. Jang, *Appl. Phys. Lett.*, 2018, **112**, 162104.

24 S.-J. Park and T.-J. Ha, *IEEE Electron Device Lett.*, 2023, **44**, 642.

25 T. Sun, L.-Q. Shi, C.-Y. Su, W.-H. Li, X.-W. Lv, H.-J. Zhang, Y.-H. Meng, W. Shi, S.-M. Ge, C.-Y. Tseng, Y.-F. Wang, C.-C. Lo and A. Lien, *SID Symp. Dig. Tech. Pap.*, 2015, **46**, 766–768.

26 I. M. Choi, M. J. Kim, N. On, A. Song, K. B. Chung, H. Jeong, J. K. Park and J. K. Jeong, *IEEE Trans. Electron Devices*, 2020, **67**, 1014–1020.

27 Y. Kikuchi, K. Nomura, H. Yanagi, T. Kamiya, M. Hirano and H. Hosono, *Thin Solid Films*, 2010, **518**, 3017–3021.

28 K. M. Niang, P. M. C. Barquinha, R. F. P. Martins, B. Cobb, M. J. Powell and A. J. Flewitt, *Appl. Phys. Lett.*, 2016, **108**, 093505.

29 J. H. Baek, H. Seol, K. Cho, H. Yang and J. K. Jeong, *ACS Appl. Mater. Interfaces*, 2017, **9**, 10904.

30 Y.-S. Shiah, K. Sim, Y. Shi, K. Abe, S. Ueda, M. Sasase, J. Kim and H. Hosono, *Nat. Electron.*, 2021, **4**, 800.

31 D.-G. Kim, J.-U. Kim, J.-S. Lee, K.-S. Park, Y.-G. Chang, M.-H. Kim and D.-K. Choi, *RSC Adv.*, 2019, **9**, 20865.

32 K. Kim, S. Jeon, H. Lee, M. Seo, H. Cho and B. Choi, *ECS J. Solid State Sci. Technol.*, 2019, **8**, Q3242.

33 G. T. Dang, T. Kawaharamura, M. Furuta and M. W. Allen, *Appl. Phys. Lett.*, 2017, **110**, 073502.

34 B. Ryu, H.-K. Noh, E.-A. Choi and K. J. Chang, *Appl. Phys. Lett.*, 2010, **97**, 022108.

35 K. H. Ji, J.-I. Kim, H. Y. Jung, S. Y. Park, R. Choi, U. K. Kim, C. S. Hwang, D. Lee, H. Hwang and J. K. Jeong, *Appl. Phys. Lett.*, 2011, **98**, 103509.

36 A. Abliz, *IEEE Trans. Electron Devices*, 2021, **68**, 3379.

37 M. Manesse, R. Sanjines, V. Stambouli, C. Jorel, B. Pelissier, M. Pisarek, R. Boukherroub and S. Szunerits, *Langmuir*, 2009, **25**, 8036.

38 J. Socratous, K. K. Banger, Y. Vaynzof, A. Sadhanala, A. D. Brown, A. Sepe, U. Steiner and H. Sirringhaus, *Adv. Funct. Mater.*, 2015, **25**, 1873.

39 C. Terrier, J. P. Chatelon, R. Berjoan and J. A. Roger, *Thin Solid Films*, 1995, **263**, 37.

40 P. Li, Z. Sa, Z. Zang, G. Wang, M. Wang, L. Liao, F. Chen and Z. Yang, *Mater. Horiz.*, 2025, **12**, 5357.

41 P. Li, H. Song, Z. Sa, F. Liu, M. Wang, G. Wang, J. Wan, Z. Zang, J. Jiang and Z. Yang, *Mater. Horiz.*, 2024, **11**, 4979.

42 Z. Zhang, X. Zhao, X. Zhang, X. Hou, X. Ma, S. Tang, Y. Zhang, G. Xu, Q. Liu and S. Long, *Nat. Commun.*, 2022, **13**, 6590.